AGU PUBLICATIONS

Paleoceanography

RESEARCH ARTICLE
10.1002/2014PA002762

Key Points:
- Methods for testing astronomically tuned age models are established
- Example data sets are used to test the methods proposed

Supporting Information:
- Texts S1 and S2
- Table S1
- Table S2
- Figure S1
- Figure S2
- R script S1
- R script S2

Correspondence to:
C. Zeeden,
c.zeeden@geo.rwth-aachen.de

Citation:
Zeeden, C., S. R. Meyers, L. J. Lourens, and F. J. Hilgen (2015), Testing astronomically tuned age models, *Paleoceanography*, *30*, 369–383, doi:10.1002/2014PA002762.

Received 26 NOV 2014
Accepted 13 MAR 2015
Accepted article online 19 MAR 2015
Published online 14 APR 2015
Corrected 23 JUL 2015

This article was corrected on 23 JUL 2015. See the end of the full text for details.

Testing astronomically tuned age models

Christian Zeeden[1,2], Stephen R. Meyers[3], Lucas J. Lourens[1], and Frederik J. Hilgen[1]

[1]Faculty of Geosciences, University of Utrecht, Utrecht, Netherlands, [2]Now at Lehrstuhl für Physische Geographie und Geoökologie, RWTH Aachen, Aachen, Germany, [3]Department of Geoscience, University of Wisconsin—Madison, Madison, Wisconsin, USA

Abstract Astrochronology is fundamental to many paleoclimate studies, but a standard statistical test has yet to be established for validating stand-alone astronomically tuned time scales (those lacking detailed independent time control) against their astronomical insolation tuning curves. Shackleton et al. (1995) proposed that the modulation of precession's amplitude by eccentricity can be used as an independent test for the successful tuning of paleoclimate data. Subsequent studies have demonstrated that eccentricity-like amplitude modulation can be artificially generated in random data, following astronomical tuning. Here we introduce a new statistical approach that circumvents the problem of introducing amplitude modulations during tuning and data processing, thereby allowing the use of amplitude modulations for astronomical time scale evaluation. The method is based upon the use of the Hilbert transform to calculate instantaneous amplitude following application of a wide band precession filter and subsequent low-pass filtering of the instantaneous amplitude to extract potential eccentricity modulations. Statistical significance of the results is evaluated using phase-randomized surrogates that preserve the power spectrum structure of the data but have randomized amplitude modulations. Application of the new testing algorithm to two astronomically tuned data sets demonstrates the efficacy of the technique and confirms the presence of astronomical signals. Additionally, it is demonstrated that a minimal tuning approach using (at maximum) one precession cycle per ~100 kyr eccentricity cycle does not introduce systematic frequency modulations, even when a narrow band-pass filter is applied, allowing direct comparison of data amplitudes and orbital eccentricity.

1. Introduction

A major improvement in constructing geological time scales has evolved from integrated stratigraphic studies in which lithostratigraphy, magnetostratigraphy, biostratigraphy, cyclostratigraphy, and radioisotopic dating are combined to establish a high-resolution astronomical tuning of climate proxy records. This approach of tying cyclic variations in the rock record to astronomical target curves has yielded geological time scales with an unprecedented accuracy, precision, and resolution. The method has resulted in, among others, the Astronomically Tuned Neogene Time Scales 2004 and 2012 (ATNTS) [*Gradstein et al.*, 2004, 2012; *Hilgen et al.*, 2012; *Lourens et al.*, 2004]; also the Paleogene part of the standard geological time scale [*Gradstein et al.*, 2004, 2012; *Luterbacher et al.*, 2004; *Vandenberghe et al.*, 2012] is largely based on an integrated stratigraphic approach, with highest fidelity for intervals based on astronomical tuning [*Luterbacher et al.*, 2004; *Vandenberghe et al.*, 2012]. Furthermore, astronomical tuning has been used to test and refine ages of mineral standards used for radioisotopic dating [e.g., *Channell et al.*, 2010; *Hilgen et al.*, 1997; *Kuiper et al.*, 2005, 2008; *Renne et al.*, 1994; *Rivera et al.*, 2011; *Westerhold et al.*, 2012; *Zeeden et al.*, 2014] to obtain more accurate radioisotopic ages via combination with cyclostratigraphic duration information [*Meyers et al.*, 2012a] and for the investigation of the Earth's climate response to astronomical insolation forcing [e.g., *Berger*, 1989; *Hays et al.*, 1976; *Holbourn et al.*, 2005; *Lourens et al.*, 2010; *Pälike et al.*, 2006b; *Ruddiman et al.*, 1986; *Shackleton*, 2000; *Meyers et al.*, 2012b].

While the application of astrochronology has fundamentally advanced our understanding of the Earth System, a standard test for validating stand-alone astronomically tuned time scales (those lacking detailed independent time control) against their astronomical insolation tuning curves has not yet been established. Such tests are not straightforward, as an appropriate null hypothesis formulation is often challenging due to practical aspects of geological data analysis, including background noise (e.g., "red noise"), complex relationships between time and stratigraphic depth, nonlinear climate/depositional system response, and circular reasoning [*Meyers et al.*, 2008; *Hilgen et al.*, 2014]. A number of statistical techniques have been

proposed to evaluate a potential astronomical imprint using either untuned depth scales or astronomically tuned time series. Among others, *Hays et al*. [1976] compared the ratio of dominant power spectral peaks in their paleoclimate data with the main periodicities of Milankovitch forcing, following the application of a simple depth-derived time scale. Also, using depth-derived time scales, *Huybers and Wunsch* [2005], *Huybers* [2007], and *Lisiecki* [2010] compared the phase of glacial terminations observed in oxygen isotope data with the phase of astronomical parameters using Rayleigh's R statistic. *Huybers* [2011] used an approach that evaluates the maxima in Milankovitch insolation forcing that occur during glacial terminations, as compared to maxima in forcing that do not coincide with terminations. Although these methods have proven successful, they require a level of detailed independent time control that is generally not afforded in pre-Pleistocene records.

To address the lack of sufficient independent time control in many deep-time records, *Meyers and Sageman* [2007] introduced the average spectral misfit (ASM) method, an approach that evaluates a range of plausible time models while simultaneously testing paleoclimate data against the expected astronomical frequencies [as in *Hays et al*., 1976]. The approach provides a formal statistical test of the null hypothesis (no astronomical signal), has been extended to evaluate stratigraphic records with unsteady sedimentation [*Meyers et al*., 2012b], and has also been adapted to evaluate astronomically tuned data [*Wendler et al*., 2014]. However, in contrast to the approaches used to test the well-dated Pleistocene records [*Huybers and Wunsch*, 2005; *Huybers*, 2007; *Lisiecki*, 2010; *Huybers*, 2011], ASM does not provide an explicit test of the linkage between an astronomical forcing curve and paleoclimate data but rather is used to test "floating" astrochronologies (for a Bayesian approach, see *Malinverno et al*. [2010]).

Shackleton et al. [1995] proposed that complex amplitude demodulation [e.g., *Bloomfield*, 2000] is a powerful tool to test for the expected eccentricity amplitude modulation (also referred to as the "instantaneous amplitude" or the "amplitude envelope") of the precession-related signal in paleoclimate records. They state that the amplitude modulation of precession is the "most important feature through which the orbital imprint may be unambiguously recognized in ancient geological records." If this is the case, the long-term amplitude variations in the theoretical eccentricity solutions (~0.4, 2.4 Myr), and in obliquity (e.g., 1.2 Myr), can be compared with their corresponding astronomical signals in paleoclimate data to support or reject proposed astronomical time scales. Such an approach has been applied in numerous studies using either amplitude variations represented by band-pass filter output [e.g., *Abels et al*., 2010; *Channell and Kleiven*, 2000; *Evans et al*., 2007; *Paillard*, 2001; *Tiedemann et al*., 1994; *Westerhold et al*., 2005, 2014; *Valero et al*., 2014] or amplitude demodulation techniques [e.g., *Clemens*, 1999; *Pälike et al*., 2001, 2004, 2006a; *Shackleton and Crowhurst*, 1997; *Westerhold et al*., 2007; *Wu et al*., 2013]. However, other studies have demonstrated that eccentricity-like amplitude variations can be artificially introduced into paleoclimate data by tuning and data processing [*Neeman*, 1993; *Huybers and Wunsch*, 2004; *Huybers and Aharonson*, 2010]. These results suggest that the amplitude modulation approach cannot be used as an independent test to test the accuracy of astronomically tuned time scales. More generally, many more studies have demonstrated how astronomical frequencies can be introduced into records by astronomical tuning [e.g., *Hilgen et al*., 2006; *Hinnov and Park*, 1998; *Rial*, 1999; *Rial and Anaclerio*, 2000; *Shackleton et al*., 1995] and standard statistical tests to decipher whether observed cycles and their amplitude modulations are real or artificial are lacking.

Here we introduce a new testing approach that circumvents the potential problem of introducing amplitude modulations during tuning and data processing, thereby allowing the use of amplitude modulations for astronomical time scale evaluation. The method involves five essential steps: (1) the application of a wide band precession filter (wide here meaning a bandwidth that is ~65% of the center frequency) to inhibit the generation of artificial amplitude modulations that mimic eccentricity, (2) application of a Hilbert transform to calculate instantaneous amplitude, (3) low-pass filtering of the instantaneous amplitude to extract potential eccentricity modulations, (4) calculation of the Spearman's rank correlation [*Spearman*, 1904] between amplitude modulations observed in the tuned data and eccentricity target series, and (5) evaluation of the statistical significance of the results using phase-randomized surrogates that preserve the power spectrum structure of the data but have randomized amplitude modulations [*Ebisuzaki*, 1997]. Application of the new method to astronomically tuned data sets from Ceara Rise (Miocene) and the Mediterranean (Pleistocene-Pliocene) demonstrates the efficacy of the technique and confirms the presence of strong astronomical signals in these records.

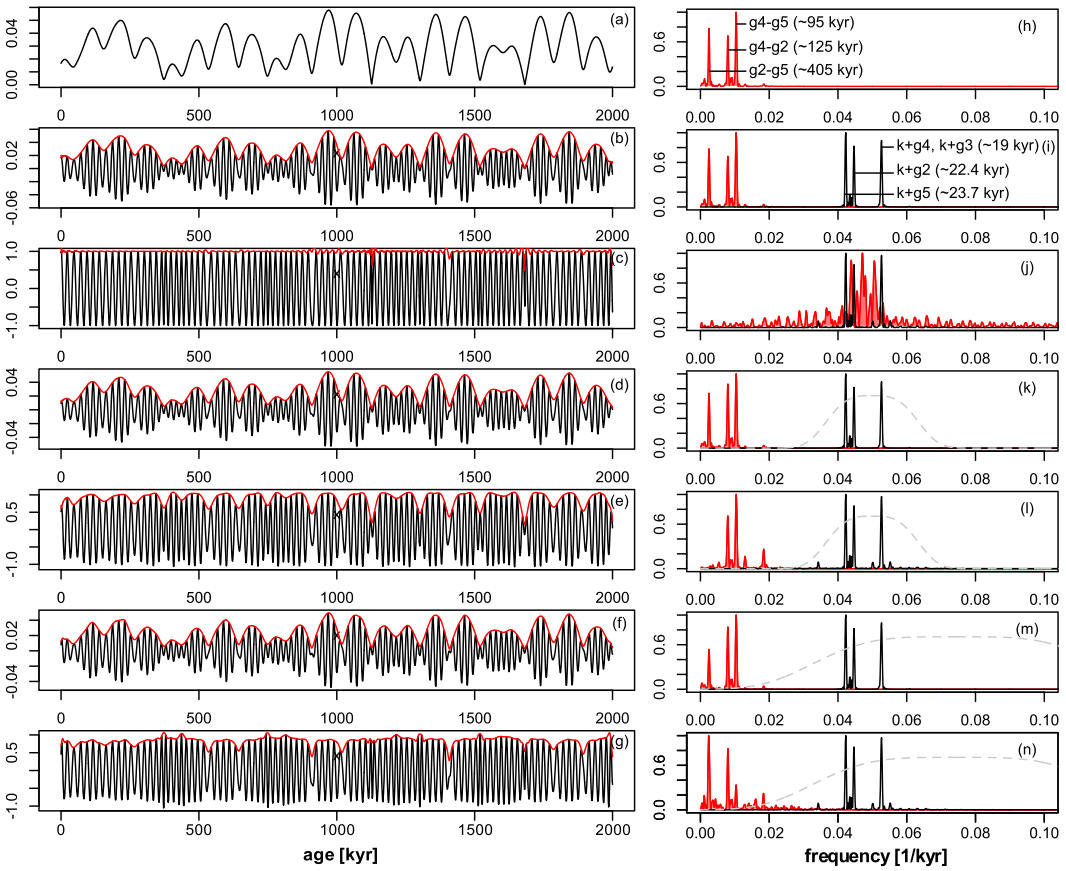

Figure 1. Analysis of the astronomical solutions from *Laskar et al.* [2004] and their amplitude modulations including (a) orbital eccentricity; (b) e*sinω, the climatic precession index; and (c) sinω, the axial precession. The (d) output from a narrow precession filter applied to e*sinω, (e) output from a narrow precession filter applied to sinω, (f) output from a broad precession filter applied to e*sinω, (g) output from a broad precession filter applied to sinω are also shown. The narrow precession filter employs a Taner filter with cutoff frequencies (half power points) at 0.035 and 0.065 cycles/kyr, and a roll-off rate of 10^4. The broad precession filter employs a Taner filter with cutoff frequencies at 0.029 and 0.12 cycles/kyr, and a roll-off rate 10^3. Instantaneous amplitude for each record, determined with a Hilbert transform, is shown in red. (h–n) The power spectra (the square modulus of the Fourier transform) for each amplitude envelope (red), along with the spectra of the prefiltered series (black) and the Taner band-pass window used (gray dashed line). To better illustrate the structure of the spectra, each power spectrum has been normalized to a maximum of unity.

2. Frequency Versus Amplitude Modulation: Properties of the Astronomical Solution

The climatic precession index, e*sinω, is defined by the product of eccentricity, e, and axial precession, sinω, where ω is the angle between Northern Hemisphere spring equinox and perihelion along the Earth's orbit. Thus, it can be seen that variations in eccentricity control the amplitude of climatic precession in quasiperiodic oscillations of (among other less influential periods) 405, 95, and 124 kyr, i.e., the three main components of eccentricity associated with the so-called resonances between fundamental frequencies g2 (Venus) minus g5 (Jupiter), g4 (Mars) minus g5 (Jupiter), and g4 (Mars) minus g2 (Venus), respectively (Figures 1a–1c) [*Laskar et al.*, 2004]. These three dominant periods of eccentricity are also expressed as the difference frequencies between the main precession periods of 23.690, 22.385, and 18.956 kyr (calculated for the past 3 Ma); the precession periods depend on geological time [*Berger et al.*, 1992a, 1992b] and parameters of the Earth-Moon system, see *Laskar et al.* [1993]. This relationship is due to the fact that the precession periods are derived from the sum frequencies between the precession constant ($\psi = 25.675$ kyr) and the fundamental frequencies g5 (Jupiter), g2 (Venus), and g4 (Mars). While eccentricity modulates the amplitude of precession, eccentricity also modulates its instantaneous frequency (for both axial precession and climatic precession), but with a notable absence of the 95 kyr component [*Hinnov*, 2000]. Of critical importance, when a relatively narrow band-pass

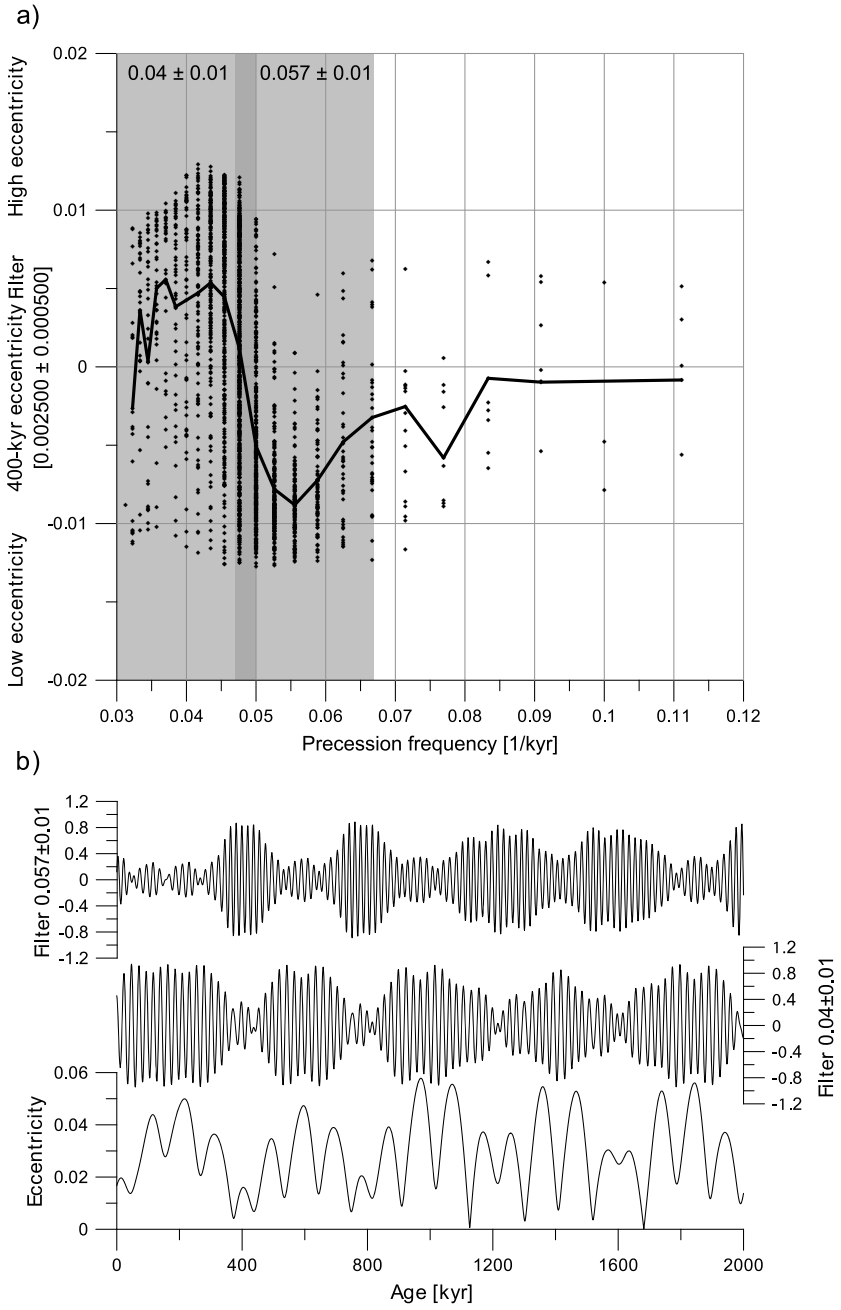

Figure 2. (a) Dependency of the 405 kyr eccentricity component (ordinate) upon the precession frequency (abscissa; bold line is the average eccentricity value for each precession frequency). Note the shift at ~0.05 cycles/kyr (corresponding to ~20 kyr); frequencies >0.05 occur predominantly during ~405 kyr eccentricity minima and vice versa. (b) To demonstrate this effect, (bottom) the eccentricity is compared to two Gaussian filters outputs from sinω (see Figure 1c) focusing on frequencies ⁑0.05. The Gaussian filtered frequencies (using the Analyseries software [*Paillard et al.*, 1996]) and their overlap are shaded gray in Figure 2a.

filter (e.g., 0.05 ± 0.015 cycles/kyr; narrow here meaning a bandwidth that is 30% of the center frequency) is applied to a precession-tuned time series—as is common practice in cyclostratigraphy—the resulting amplitude modulation may either represent the true amplitude modulation or may be generated by interactions between the band-pass filter and the frequency modulation imposed during tuning. As a test case to demonstrate this effect, *Huybers and Aharonson* [2010] analyzed an axial precession (sinω) time series (Figures 1c and 1j), because it does not contain the eccentricity amplitude modulation (in contrast

to the climatic precession index; Figures 1b and 1i). The eccentricity-related amplitude modulation observed in the filtered axial precession time series (Figure 1e) looks similar to the one from the climatic precession index (Figure 1d; Spearman's rank correlation = 0.74), thereby suggesting that the presence of eccentricity-like amplitude modulation in precession-filtered records does not support the accuracy of astronomically tuned time scales [*Huybers and Aharonson*, 2010].

The average period of precession is 21.1 kyr, but the distribution of observed precession frequencies in the theoretical solution [*Laskar et al*., 2004] varies over a full ~405 kyr eccentricity cycle (e.g., Figure 1d of *Meyers and Hinnov* [2010] and Figure 2 of *Huybers and Aharonson* [2010]). Importantly, the distribution of frequencies is not symmetric over an ~405 kyr cycle. To illustrate this characteristic, Figure 2 plots the local precession frequency (represented by the inverse of time between successive precession minima and successive precession maxima), as a function of the ~405 kyr eccentricity component over the past 25 Ma (Figure 2a). It is apparent that relatively long (>20 kyr; frequency <0.05 cycles/kyr) precession cycles occur predominantly during ~405 kyr eccentricity maxima, whereas short (<20 kyr; >0.05 cycles/kyr) precession cycles predominantly occur during ~405 kyr eccentricity minima. This characteristic is further demonstrated by Gaussian band-pass filtering [*Paillard et al*., 1996] of the precession (sinω) signal, focusing on frequencies above or below 0.05 cycles/kyr (Figure 2b). For the higher-frequency ranges of precession (i.e., >0.05 cycles/kyr), we observe an opposite amplitude phasing relative to the (405 kyr) eccentricity cycle (Figure 2b). This relationship originates from the highest-amplitude precession frequencies <0.05 cycles/kyr (1/23.690 kyr; $\psi + g5$ and 1/22.385 kyr; $\psi + g2$) being responsible for the ~405 kyr eccentricity amplitude modulation. A dominance of the frequencies <0.05 during eccentricity maxima and low amplitudes during ~405 kyr minima leads to a relative high contribution of the >0.05 cycles/kyr frequency components (1/18956 kyr; $\psi + g4$ and 1/19097 kyr; $\psi + g3$) during ~405 kyr eccentricity minima.

3. Approaches to Test Astronomically Tuned Time Series

3.1. Testing Tuned Data Sets

Motivated by the method of *Shackleton et al*. [1995], and subsequent challenges to the amplitude modulation approach [*Huybers and Aharonson*, 2010], we develop a new technique to test astronomically tuned time series. Our goal is to circumvent the potential problem of introducing amplitude modulations during tuning and data processing, thereby allowing the use of amplitude modulations for astronomical time scale evaluation. Since the key shortcoming identified in prior studies arises from artifacts associated with the use of a narrow band-pass filter, we begin by considering filter design. Two central questions that we will contemplate are as follows: (1) Can we design a filter (or a series of filters) that allows us to distinguish between true eccentricity-related amplitude modulation and tuning-induced modulation? (2) Related to this, can we leverage filter "artifacts" (distortion of the amplitude modulations by the filter) to discern true eccentricity-related amplitude modulation?

To begin our investigation, we extract the precession components of the axial and climatic precession time series over the past 2 Ma at frequencies of 0.05 ± 0.015 (cycles/kyr) and 0.0745 ± 0.0455 (cycles/kyr), corresponding to ~15.4–28.6 kyr and ~8.3–34.5 kyr, using a Taner band-pass filter [*Taner*, 1992] (Figure 1). A Hilbert transformation is applied to quantify the amplitude modulations ("instantaneous amplitude"; e.g., Figures 1d–1g) in the filtered time series. When a relatively narrow filter is used, i.e., ~15.4–28.6 kyr, both time series display a similar instantaneous amplitude pattern (Figures 1d and 1e); note that the 405 kyr amplitude variations are more pronounced in the filtered e*sinω (Figures 1d and 1k) than in the filtered sin ω (Figures 1e and 1l). However, when the bandwidth of the filter is increased, thereby including all periods between ~8.3 and 34.5 kyr, marked differences occur between the time series. The filtered climatic precession time series still displays the original amplitude modulation (Figure 1f), whereas that of axial precession displays weaker fluctuations of the amplitude with overall highest amplitudes during eccentricity minima (Figure 1g).

It is useful to evaluate the power spectrum characteristics of these time series (Figures 1h–1n). Comparison of the power spectra of the amplitude envelopes demonstrates that the 95 kyr, 124 kyr, and 405 kyr eccentricity components are not present in sinω (Figure 1j), although eccentricity cycles emerge when a narrow band-pass filter is applied (Figure 1l). A notable difference is the loss of the 405 kyr signal and the appearance of an ~54 kyr cycle (0.0184 cycles/kyr; Figure 1l), although there still exists a strong correlation of

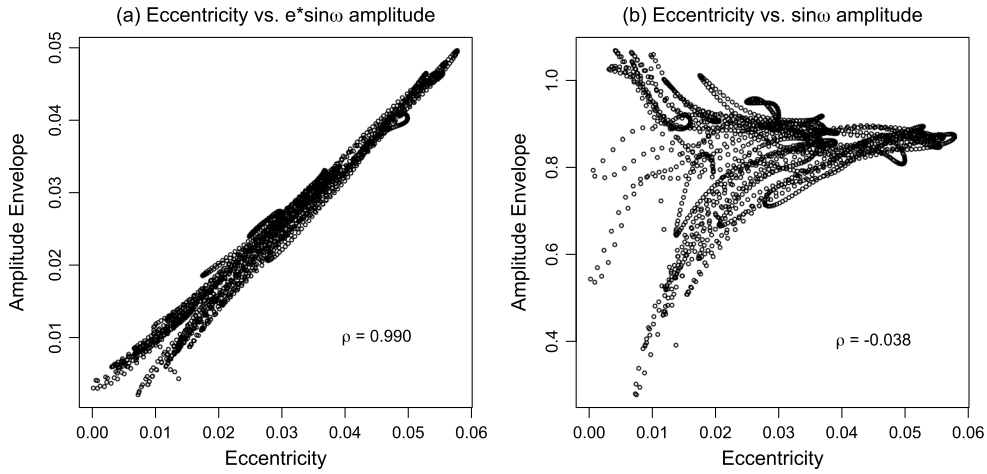

Figure 3. Crossplot of the theoretical eccentricity series [*Laskar et al.*, 2004] versus the amplitude envelope determined following application of a broad precession filter for (a) esinω and (b) sinω. The degradation of correlation in Figure 3b indicates that this filter can be used as a diagnostic tool for identifying true versus induced amplitude modulation. Parameter ρ represents results from Spearman's rank correlations.

the amplitude modulations (Figure 1e) with eccentricity (Figure 1a; Spearman's rank correlation = 0.72). When a broad band-pass filter is applied, we observe a marked change in the spectral response between sinω (Figure 1m) and e*sinω (Figure 1n): the power maxima of the 405 kyr, 124 kyr, and 95 kyr peaks successively increase for e*sinω but decrease for sinω. It is this opposite response in power, and associated changes in phase, that ultimately result in a poor correlation between the filtered sinω amplitude envelope and eccentricity (Figure 3; Spearman's rank correlation = −0.038), providing a diagnostic tool for the identification of true eccentricity-related amplitude modulations.

Thus, it is clear that the application of a broad band-pass filter (~8.3–34.5 kyr), followed by calculation of instantaneous amplitude, can distinguish between actual and induced amplitude modulations in the models (Figures 1f and 1g). However, the presence of geologic and climate noise (including sedimentation rate changes and "red noise" [*Meyers and Sageman*, 2007; *Meyers*, 2012]) yields more complex spectra and makes this simple approach of limited practical utility in real paleoclimate data. The overall effect of such noise is to add frequency content within the filter bandwidth, in excess of that expected from the precession forcing, which ultimately distorts the instantaneous amplitude result. However, if this noise contribution is not too large, the expected eccentricity amplitude modulations are preserved in the low-frequency variability of the instantaneous amplitude result, although mixed with the noise. Application of a low-pass filter (a Taner filter with cutoff frequency of 0.013 cycles/kyr and a roll-off rate of 10^4) to the instantaneous amplitude output allows extraction of the eccentricity modulations, if they are truly present in the paleoclimate data. If designed appropriately, the low-pass filter can also help to offset the distortions introduced from the broad filter (compare the red spectra in Figures 1i and 1m). It is important to note that the specific characteristics of the precession and low-pass filters used here have been carefully chosen to optimize the detection of eccentricity modulations, but many other possible filter designs are possible, and this remains a worthwhile avenue of inquiry.

To provide a quantitative measure of fit, correlation between theoretical eccentricity and the filtered (data) instantaneous amplitude is determined using the Spearman's rank correlation coefficient, which allows for a degree of nonlinearity between the records. To accommodate potential distortion of the theoretical eccentricity series by the data processing algorithm, e*sinω is processed using an identical approach as the data to generate the eccentricity target used for comparison. Evaluation of the statistical significance of correlation between the low-pass filtered e*sinω amplitude and the low-pass filtered data amplitude is conducted via Monte Carlo simulation [*Ebisuzaki*, 1997]. Each simulation has an identical power spectrum to the paleoclimate data but has randomized phase. There are several desirable properties of this approach: (1) the phase-randomized surrogates preserve the same exact autocorrelation structure (e.g., autoregressive

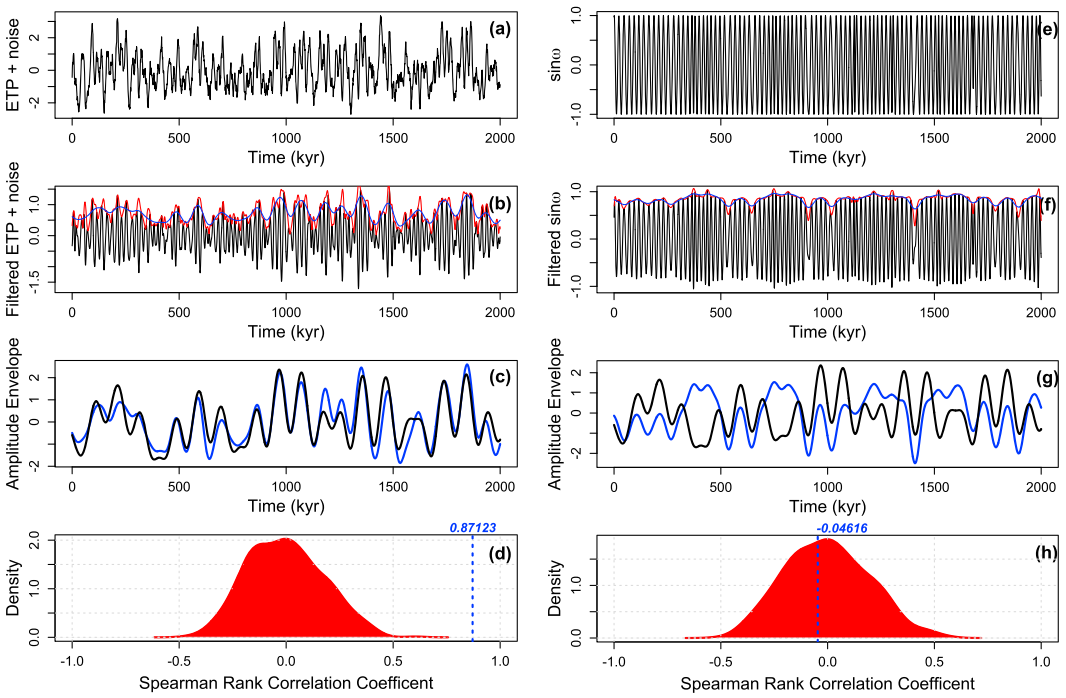

Figure 4. Demonstration of the complete algorithm as applied to a (a–d) normalized eccentricity-tilt-precession (ETP) series with red noise and (e–h) axial precession. The ETP series was created by giving equal power to each component, followed by normalization of the total ETP signal to unit variance, and the addition of red noise with $\rho = 0.9$ (scaled to have a variance of 0.25). (Figure 4a) ETP model series. (Figure 4b) ETP model filtered with a broad precession filter (black), its instantaneous amplitude (red), and the final amplitude envelope following application of a low-pass filter (blue). (Figure 4c) Comparison of the final ETP model amplitude envelope (blue) and the amplitude envelope for esinω (black; processed using the same filtering algorithm). (Figure 4d) Kernel density estimate of Spearman's rank correlation coefficients for the phase-randomized surrogate simulations, and the observed correlation coefficient for the ETP model (blue line). Monte Carlo simulation yields a *P* value of <0.01 for the ETP Spearman's rank correlation coefficient and a *P* value of 0.871 for the e*sinω Spearman's rank correlation coefficient. (Figures 4e–4h) Follow the same format but for axial precession.

red noise) as the paleoclimate data and (2) since the character of the amplitude modulation depends upon phase, randomizing phase will produce random modulations for each simulation. Comparison of the observed data correlation (r_{data}) with those from Monte Carlo simulations (r_{sim}) allows a rigorous evaluation of the null hypothesis (no correlation between eccentricity target and observed modulations). As in *Ebisuzaki* [1997], the reported *P* value is estimated by determining the fraction of simulation correlations that have a magnitude ($|r_{sim}|$) greater than that of $|r_{data}|$. Importantly, this testing approach is legitimate even when a comprehensive precession-scale tuning is conducted.

We have also investigated the use of AR1 surrogates for the evaluation of statistical significance. While AR1 surrogates do not have the two desirable properties noted above, they can preserve a correlation in phase between adjacent frequencies, as may be expected in red noise. Evaluation of the two approaches via numerical experiments (not shown) indicates that the phase-randomized surrogate method provides a more demanding test of the null hypothesis, and thus this approach is preferred in the present study.

The full algorithm is outlined in Figure 4, with results for sinω, and for a normalized eccentricity-tilt-precession (e sinω) model, the latter of which includes contributions from red noise. The results illustrate the reliability of the method in identifying true eccentricity modulation of precession, even when strong obliquity signals are present. In cases where no simulations ($|r_{sim}|$) achieve the observed $|r_{data}|$, such as in Figure 4d, we recommend that the *P* value be reported as $<1/N*10$, where *N* represents the number of simulations. A factor of 10 is included to make a conservative statement about the simulation experiment, which by its nature yields different results in every experimental run.

In order to apply this approach, time series require a high enough resolution to allow for the identification and filtering of hypothesized precession signals and a length sufficient to characterize the eccentricity-scale modulation. When investigating short (e.g., "only" 500 kyr long) time series, the odds are higher to find a surrogate resembling eccentricity than for longer records; thus, the statistical power of the method is lower, and false negatives are more likely. Under such circumstances, extension of the record may help to resolve this issue, if a strong precession signal is indeed preserved.

To facilitate the use of this method, a function ("testPrecession") that conducts the full analysis has been developed for "astrochron: An R Package for Astrochronology" [*Meyers*, 2014].

3.2. Minimal Tuning (Using One Tie Point per ~100 kyr Cycle) Does not Introduce Frequency Modulations

An additional approach to evaluate the robustness of the astronomical tuning is to apply a minimum number of calibration points ("minimal tuning"). Ideally, the data set should be tuned to 405 kyr eccentricity only, as this will not transpose individual precession frequencies onto a tuned data set but only the average precession frequency. However, since sedimentation rates may change considerably over such time spans, and the *precise* (precession cycle-scale) location of minima and maxima of the ~405 kyr eccentricity are sometimes challenging to identify in real data sets, here we focus on the ~100 kyr eccentricity cycle. To test whether a frequency modulation can be introduced by tuning a simple (nonmodulated) cyclic signal to every ~100 kyr eccentricity maximum, we (1) generate a sine function with a 20 kyr period spanning 4 Ma, (2) identify the theoretical eccentricity maximum [*Laskar et al*., 2004] that is closest to the maximum of each 20 kyr cycle, (3) use these as tie points for tuning to eccentricity maxima, and (4) plot the new "tuned" frequency versus eccentricity (Figure S1 in the supporting information). The analysis indicates that such an approach does not introduce systematic frequency modulations (see Figure S1 in the supporting information). Thus, the amplitude envelope of data tuned to ~100 kyr eccentricity cycles (or to about every 5th precession cycle only) can be evaluated without the problem of introducing precession frequency modulation during the tuning process, even when a narrow band-pass filter is applied. We use a "100 kyr minimal tuning" approach to supplement the method outlined in section 3.1. This approach also leverages off the fact that, in many cases, sedimentary precession cycles can be better recognized during eccentricity maxima than during eccentricity minima.

4. Testing Astronomically Tuned Time Scales

As test cases for the new testing approach, we investigate two astronomically tuned records to determine if eccentricity amplitude modulation is truly present or if it may derive from frequency modulation introduced by the tuning and the data processing procedure. These time scales comprise (1) the Mediterranean Pliocene (Ocean Drilling Program (ODP) Site 967) between 2.3 and 3.2 Ma [*Lourens et al*., 2001a, 2001b] and (2) the Miocene of Ceara Rise (Ocean Drilling Program (ODP) Site 926) between 8 and 10 Ma [*Zeeden et al*., 2013a, 2013b].

4.1. Astrochronology of the Eastern Mediterranean Pliocene

ODP Site 967 [*Emeis et al*., 1996; *Robertson et al*., 1998] contains a unique data set that has been interpreted to represent astronomically driven northern African humidity changes [*Lourens et al*., 2001a]. Humidity changes are inferred from variations in the ratio of titanium (Ti) versus aluminum (Al) of its bulk sediment composition (Figure 5), with high Ti concentrations corresponding to increased dust input from the Sahara region and high Al concentrations due to enhanced runoff from the Nile River [*Wehausen and Brumsack*, 2000]. In 2001 (a), *Lourens et al*. used this high-quality record with a temporal resolution of ~2 kyr to constrain the tidal dissipation and/or dynamical ellipticity values of the Earth that were incorporated in the La90 astronomical solution [*Laskar*, 1990; *Laskar et al*., 1993]. For this purpose, they tuned each minimum and maximum in the Ti/Al record to their inferred p-0.5 t minimum and maximum [*Lourens et al*., 2001a], based on an initial biostratigraphic age model. P-0.5 t denotes a mix of precession and tilt (obliquity), where the tilt component has half the precession amplitude; the pattern of p-0.5 t mimics that of the 65°N summer insolation curve [*Lourens et al*., 1996a]. The originally published Ti/Al data have been subsequently extended [*Lourens et al*., 2001b] and tuned in the same manner to ~3.2 Ma, and we have updated the time scale to the newer La2004

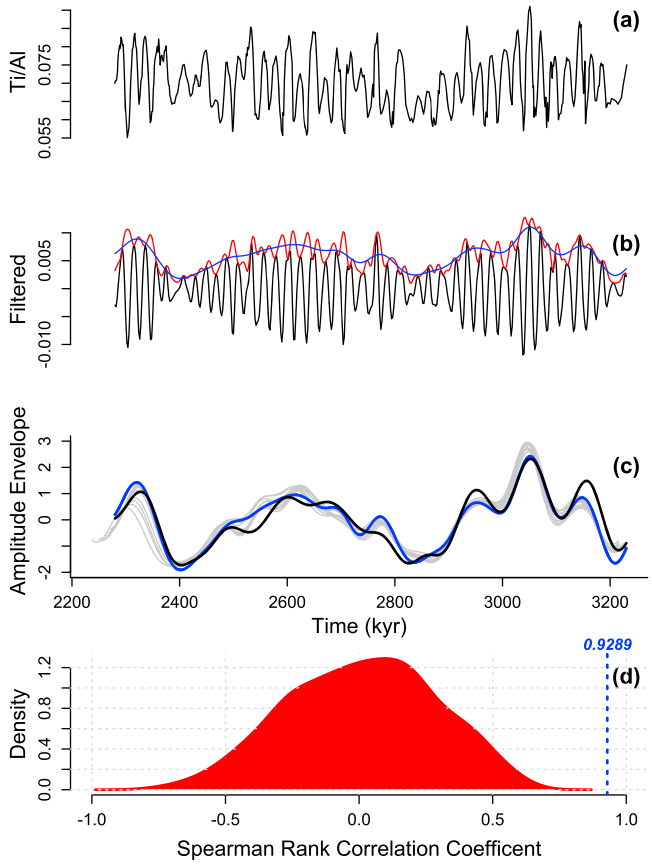

Figure 5. Evaluation of the astronomically-tuned Site 967 Ti/Al data from the Mediterranean Sea [*Lourens et al.*, 2001b]. (a) Ti/Al data series with interpreted 100 and 405 kyr high-precession-amplitude clusters. (b) Ti/Al data filtered with a broad precession filter (black), its instantaneous amplitude (red), and the final amplitude envelope following application of a low-pass filter (blue). (c) Comparison of the final Ti/Al amplitude envelope (blue) and the amplitude envelope for e*sinω (black; processed using the same filtering algorithm), as well as the results for the 10 minimally tuned series (gray). For plotting purposes, all data series have been standardized (zero mean, unit standard deviation). (d) Kernel density estimate of Spearman's rank correlation coefficients for the phase-randomized surrogate simulations and the observed correlation coefficient for the Site 967 Ti/Al data (blue line). Note that the kernel density estimate is a visualized simplification of the simulations.

solution [*Laskar et al.*, 2004], even though age differences between the La90 and La2004 are small for this interval of time. Tuning tie points are available in the supporting information.

Following the well-established late Pleistocene phase relations between Mediterranean climate changes (i.e., sapropel formation) and astronomical forcing [*Hilgen*, 1991; *Lourens et al.*, 1996b], the tuned Ti/Al record suggests two large-scale clusters of 10–15 prominent precession cycles, marking the imprint of the 405 kyr eccentricity period (Figure 5a). In addition, three smaller groups of 3–4 prominent precession cycles are suggested in the lowest large-scale cluster and one in the topmost part of the record, which correspond to the expected 95–125 kyr eccentricity modulation. The interference between precession and obliquity forcing is also apparent by the alternation of high and low Ti/Al maxima and minima, especially in the upper/younger large-scale cluster [*Lourens et al.*, 2001a]. Hence, the distinct visibility of the eccentricity-modulated precession amplitudes in the raw data record—prior to filtering—is good qualitative evidence for their veracity.

To provide a quantitative evaluation of the Site 967 Ti/Al modulations, including a statistical evaluation of the null hypothesis, we apply the new algorithm (Figure 5). The visual match between the theoretical eccentricity tuning curve and filtered instantaneous amplitude (Figure 5c) is striking, and the records achieve a Spearman's rank correlation coefficient of 0.93 (Figure 5d). Monte Carlo simulation using 1000 phase randomized surrogates yields a P value of <0.01 (Figure 5d), none of the random simulations achieve $|r_{sim}|$ values as large as that observed in the Site 967 Ti/Al data. This provides strong quantitative evidence for the presence of precession and eccentricity signals and supports the astrochronologic model of *Lourens et al.* [2001a].

To supplement this analysis, we also used a minimal tuning approach, where the Ti/Al record was tuned to every 10th tie point only. For all 10 resulting tuning options (5 for p-0.5 t minima and maxima each), the complete analysis above was performed. The results are almost identical to the original fully tuned Ti/Al time series (see Figure 5).

4.2. Testing the Miocene Ceara Rise Record

Excellent high-resolution records of astronomically driven past climatic fluctuations have been recovered from the equatorial Atlantic during ODP Leg 154 [e.g., *Curry et al.*, 1995; *Pälike et al.*, 2006a; *Shackleton et al.*,

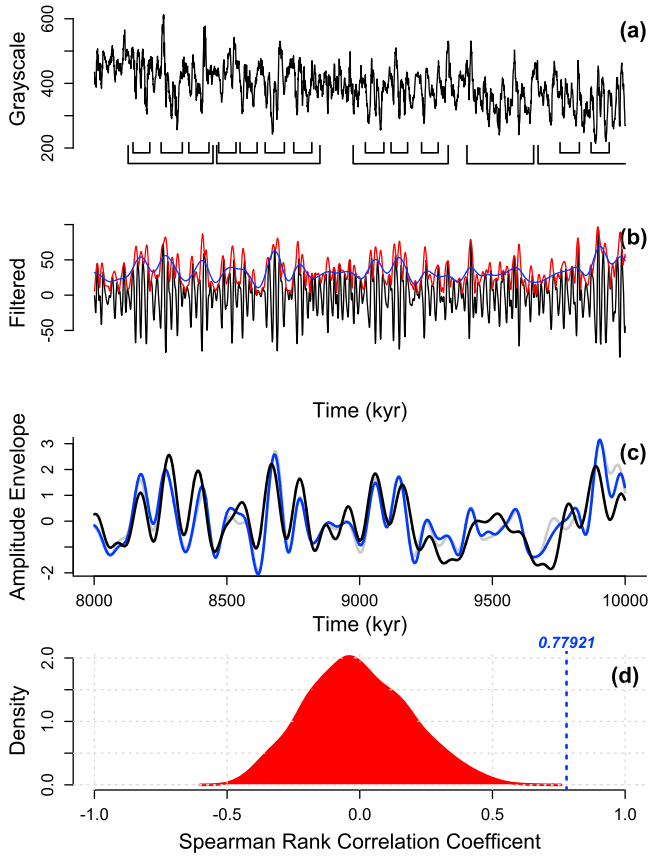

Figure 6. Evaluation of the astronomically tuned Site 926 gray scale data from the equatorial Atlantic. (a) Gray scale data series, including interpreted 100 and 405 kyr high-precession-amplitude clusters. (b) Gray scale data filtered with a broad precession filter (black), its instantaneous amplitude (red), and the final amplitude envelope following application of a low-pass filter (blue). (c) Comparison of the final gray scale amplitude envelope (blue), the amplitude envelope for e*sinω (black; processed using the same filtering algorithm), and the results tuning to every 5th cycle (light gray). For plotting purposes, all data series have been standardized (zero mean, unit standard deviation). (d) Kernel density estimate of Spearman's rank correlation coefficients for the phase-randomized surrogate simulations and the observed correlation coefficient for the Site 926 gray scale data (blue line).

1997, 2000; *Zachos et al*., 2001], and cyclostratigraphy can be continuously applied from the recent into the Miocene. The astronomically tuned time scale constructed for ODP Leg 154 Sites [*Shackleton and Crowhurst*, 1997] forms the backbone of the (equatorial Atlantic) Miocene biostratigraphy [*Backman and Raffi*, 1997; *Turco et al*., 2002]. The tuning was later updated to the La2004 solution [*Lourens et al*., 2004; *Raffi et al*., 2006] and recently revised for the interval between 5 and 14.4 Ma [*Zeeden et al*., 2013a]. *Zeeden et al*. [2013a] tuned (almost) every p-0.5 t maximum to gray scale minima and maxima of the magnetic susceptibility. Here we focus on the interval between 8 and 10 Ma in the tuned gray scale record (Figure 6a), which suggests the expression of an eccentricity-related bundling of ~5 (i.e., 95–125 kyr eccentricity) and ~20 (i.e., 405 kyr eccentricity) precession-controlled lithological cycles; these patterns are also observed in core photographs and physical property records [*Shackleton and Crowhurst*, 1997; *Zeeden et al*., 2013a].

The eccentricity-related bundling of cycles is more apparent in some intervals than in others (Figure 6a and Figure 3 of *Zeeden et al*. [2013a]). The hypothesized precession cycles are prominently developed between ~9.4 and 9.65 Ma, but they lack a clear bundling. This aberrant pattern is interpreted as reflecting an ~405 kyr eccentricity maximum within a long-term 2.4 Myr eccentricity minimum, comparable to the pattern shown for the Mediterranean Ti/Al record around 2.6 Ma (Figure 5a). This long-term eccentricity minimum also appears in the astronomical solution and could therefore be used as a first-order calibration step in the tuning procedure. Since the lithological cycles suggest an eccentricity-related amplitude modulation, it is likely that the tuned physical property data also primarily reflect true amplitude variations, as suggested by *Shackleton and Crowhurst* [1997].

Application of the new testing algorithm to the high-resolution gray scale data [*Zeeden et al*., 2013b] indicates an overall good visual match between the low-pass filtered instantaneous amplitude and theoretical eccentricity tuning curve (Figure 6c). A notable exception is the interval from 9300 to 9600 kyr, when the ~100 kyr component of eccentricity is weak. The Spearman's rank correlation coefficient is 0.78, reduced compared to the estimate from the Site 967 Ti/Al data, largely due to this short interval of misfit. Monte Carlo simulation using 1000 phase randomized surrogates yields a P value of <0.01 (Figure 6d), and none of the random simulations achieve $|r_{sim}|$ values as large as that observed in the Site 926 gray scale data. This provides strong quantitative evidence for the presence of precession and eccentricity signals and supports the astrochronologic model of *Zeeden et al*. [2013a].

In a second step, we apply the minimal tuning approach by reducing the number of tie points to one fifth of the original number (i.e., to about every 5th p-0.5 t cycle). Application of the testing algorithm indicates reproduction of the eccentricity pattern very well, except again, for the interval between 9300 and 9600 ka (Figure 6c). The Spearman's rank correlation coefficient for this minimally tuned record is 0.73, with a *P* value of <0.01. Hence, precession-filtered amplitude variations show a consistent, i.e., an in-phase relationship with the 405 kyr component of eccentricity, thereby supporting the tuning on at least the eccentricity scale.

Overall, we find that the correlation between data amplitudes and eccentricity is related to the standard deviation of eccentricity; the data amplitudes show a good fit with eccentricity especially where the 100 kyr cyclicity is pronounced, while the fit is generally less good in intervals where the 100 kyr cyclicity is weak as in the case of long-term eccentricity minima (Figure S2 in the supporting information). During such minima, amplitude variations in data are often small and detected amplitudes are more easily affected by noise/distortion. Further, nonlinear responses of sedimentary systems to insolation forcing may lead to a different sedimentary (cyclic) response during eccentricity minima and maxima, which may complicate results. Such nonlinear responses can be observed in numerous records, and sedimentation models reproduce such features [*Fischer et al*., 1991; *Ripepe and Fischer*, 1991]. As a consequence, intervals of high eccentricity should preferentially be interpreted.

5. Discussion

For the evaluation of geological data, relatively narrow precession filters are often applied to avoid the effects of noise and contributions from the ~29 kyr obliquity component; also, interference between precession (and obliquity) components may lead to a weak ~29 kyr component [*von Dobeneck and Schmieder*, 1999]. It has been previously demonstrated that tuning and filtering with such narrow filters can imprint artificial similarity between the amplitude modulation of the data and eccentricity, an attribute that is often used to test the veracity of astrochronologies [e.g., *Shackleton et al*., 1995; *Huybers and Aharonson*, 2010]. In this study, a series of filters (including a relatively wide precession filter) are used to circumvent the problem of introducing artificial amplitude modulations during tuning and data processing. We demonstrate the method with models and through the evaluation of two tuned data series. The example shown in Figure 4, using a normalized eccentricity-tilt-precession model, indicates that the wide filter (including the ~29 kyr obliquity component) performs well even when a strong obliquity signal is present.

It is critical to note that in our assessment of data sets from the Pliocene and Miocene, the specific tuning options investigated may not be the only ones that would result in a statistically significant relationship. However, a good fit of the data amplitude envelope and eccentricity (or long-term obliquity) probably does not allow for a shift in tuning by several cycles. Misfit between data and tuning target may be the result of stratigraphical issues, changing sedimentation rates, noisy data, and/or a nonconstant response to orbital forcing over time. In most cases, detailed data analysis can likely give insight into reasons for the misfit. The cross correlations quantified here reflect how much variation is shared between the data series amplitude envelope and the tuning target; even when this correlation is low, cycle counting (if done carefully) can potentially have a higher resolution than might be expected based on the correlation coefficient.

In cases of highly variable sedimentation rates, where a comprehensive precession-scale tuning is needed, the full testing algorithm (with a series of filters) is generally required. For records with relatively uniform sedimentation rates, a simpler 100 kyr minimal tuning may perform reliably, even when a narrow band-pass filter is utilized. However, records showing a systematic relation between long-term astronomical forcing and sedimentation rates (e.g., eccentricity; see *van der Laan et al*. [2005] for an example) may be less problematic for the 100 kyr minimal tuning approach, depending on the magnitude of sedimentation rate changes. In such cases, the orbital forcing (precession amplitude/eccentricity) is, however, evaluated against a stretched/compressed sedimentary signal complicating the interpretation.

In principle, the methods discussed above for precession can be applied to evaluate obliquity as well. However, a minimal tuning approach for obliquity may be difficult in practice, because tuning to the long-term obliquity amplitude variation (~1.2 Ma) is not very helpful in records with variable sedimentation rates. Tuning to one cycle per ~180 kyr obliquity amplitude variation cycle may be possible in cases where this modulation appears to be visible in data. Another approach is to only use tie points every ~5th proposed obliquity cycle.

The astronomical solutions can be reliably calculated to ~50 Ma [*Laskar et al*., 2004, 2011; *Westerhold et al*., 2012]; thus, the testing methods described here can be applied to test astrochronologies for most of the Cenozoic. However, *Shackleton et al*. [1995] note that amplitude demodulation is not always applicable to evaluate paleoclimate time series but requires data showing a strong/dominant signal in the frequency to be analyzed. When both strong precession and obliquity are present in a paleoclimate record, demodulation results from both terms provide the opportunity for cross validation. This approach is also complimentary because precession amplitudes may be especially weak during eccentricity minima, while obliquity signals are often obvious at this time [e.g., *Hilgen et al*., 1995, 2003; *Zeeden et al*., 2013a].

Finally, evaluation of the sedimentation rates resulting from the tuning procedure provides an additional means to qualitatively evaluate the plausibility of an astrochronology. Relatively constant, or slowly varying, sedimentation rates can be interpreted as the result of a reasonable tuning—but the specific tuning applied may not be the only viable option. Alternatively, large jumps in sedimentation rates may either be the result of true sedimentation rate variability or may result from tuning "cycles" that are actually not equally spaced in time (e.g., tuning noise to an astronomical target). Additionally, geological records may not be continuous representations of past climates, stratigraphic gaps may be present, and drilling may not allow for complete recovery of records. It has also been shown that splicing of multiple cores sometimes leads to stratigraphic complications requiring correction [e.g., *Evans et al*., 2004; *Westerhold and Röhl*, 2006, 2009]. It is particularly useful to apply time-frequency methods to the untuned depth data to evaluate these types of issues [*Meyers et al*., 2001; *Malinverno et al*., 2010; *Meyers et al*., 2012b].

In summary, the astrochronologic testing approach that is introduced in this study permits a robust evaluation of the correlation between tuned data amplitude envelopes and those of an astronomical tuning target. This method is independent from—and complementary to—power spectrum-based approaches. Thus, it is not subject to the potential shortcomings and biases previously identified in evaluation of power spectra [*Vaughan et al*., 2011; *Vaughan et al*., 2014; *Meyers*, 2012] while also overcoming identified shortcomings in amplitude modulation assessment [*Neeman*, 1993; *Huybers and Wunsch*, 2004; *Huybers and Aharonson*, 2010].

6. Conclusions

This study develops methodologies to circumvent the introduction of amplitude modulations by astronomical tuning and data processing, allowing the use of these amplitude variations to support or invalidate astronomically tuned records. We introduce a new quantitative statistical technique that employs the Hilbert transform and a series of filters to reliably extract true eccentricity amplitude modulations from precession signals in paleoclimate data. The method also includes Monte Carlo simulation to evaluate the null hypothesis of no correlation between observed data amplitude modulation and the theoretical eccentricity modulation. This new approach is supplemented by the demonstration that a minimal tuning approach (e.g., tuning to every ~5th precession cycle only) does not artificially introduce eccentricity-like amplitude modulation. A quantitative comparison of precession amplitude variability, as derived from filtering precession-dominated geological data, and the theoretical eccentricity signal, can thus be used to support a tuning, as demonstrated through our analysis of synthetic models and two astronomically tuned data sets.

Acknowledgments

The research leading to these results has received funding from the European Community's Seventh Framework Programme ([FP7/2007-2013] under grant agreement no. 215458 and was also supported by the U.S. National Science Foundation (award EAR-1151438 to S.R.M.)). A European Science Foundation (ESF Earthtime) grant facilitated travel and collaboration. Mathieu Martinez and two anonymous reviewers are thanked for constructive suggestions, which helped to improve this manuscript. This study uses solely published data, which can be found in the Pangaea open database at http://www.pangaea.de and at http://www.imcce.fr/Equipes/ASD/insola/earth/online/. A function that conducts the full analysis (testPrecession) has been developed for astrochron: An R Package for Astrochronology [*Meyers*, 2014].

References

Abels, H., H. Aziz, W. Krijgsman, S. Smeets, and F. Hilgen (2010), Long-period eccentricity control on sedimentary sequences in the continental Madrid Basin (middle Miocene, Spain), *Earth Planet. Sci. Lett.*, *289*(1), 220–231, doi:10.1016/j.epsl.2009.11.011.

Backman, J., and I. Raffi (1997), Calibration of Miocene nannofossil events to orbitally tuned cyclostratigraphies from Ceara Rise, in *Proc. ODP, Sci. Results*, vol. 154, pp. 83–100, Ocean Drilling Program, College Station, Tex.

Berger, A. (1989), Pleistocene climatic variability at astronomical frequencies, *Quat. Int.*, *2*, 1–14, doi:10.1016/1040-6182(89)90016-5.

Berger, A., M. F. Loutre, and J. Laskar (1992a), Stability of the astronomical frequencies over the Earth's history for Paleoclimate studies, *Science*, *255*, 560–566, doi:10.1126/science.255.5044.560.

Berger, A., M. F. Loutre, and V. Dehant (1992b), Pre-Quaternary Milankovitch frequencies, *Nature*, *342*, doi:10.1038/342133b0.

Bloomfield, P. (2000), *Fourier Analysis of Time Series: An Introduction*, edited by V. Barnett et al., Wiley-Interscience, Hoboken, N. J.

Channell, J., and H. Kleiven (2000), Geomagnetic palaeointensities and astrochronological ages for the Matuyama Brunhes boundary and the boundaries of the Jaramillo Subchron: Palaeomagnetic and oxygen isotope records from ODP Site 983, *Philos. Trans. R. Soc. London, Ser. A*, *358*(1768), 1027–1047, doi:10.1098/rsta.2000.0572.

Channell, J., D. Hodell, B. Singer, and C. Xuan (2010), Reconciling astrochronological and 40Ar/39Ar ages for the Matuyama-Brunhes boundary and late Matuyama Chron, *Geochem. Geophys. Geosyst.*, *11*, Q0AA12, doi:10.1029/2010GC003203.
Clemens, S. (1999), An astronomical tuning strategy for Pliocene sections: Implications for global-scale correlation and phase relationships, *Philos. Trans. R. Soc. London, Ser. A*, *357*(1757), 1949–1973, doi:10.1098/rsta.1999.0409.
Curry, W. B., et al. (1995), *Proc. ODP, Init. Rep.*, vol. 154, Ocean Drilling Program, College Station, Tex., doi:10.2973/odp.proc.ir.154.1995.
Ebisuzaki, W. (1997), A method to estimate the statistical significance of a correlation when the data are serially correlated, *J. Clim.*, *10*, 2147–2153, doi:10.1175/1520-0442(1997)010<2147:AMTETS>2.0.CO;2.
Emeis, K.-C., et al. (1996), *Proc. ODP, Init. Rep.*, vol. 160, Ocean Drilling Program, College Station, Tex., doi:10.2973/odp.proc.ir.160.1996.
Evans, H., T. Westerhold, and J. Channell (2004), ODP Site 1092: Revised composite depth section has implications for Upper Miocene' cryptochrons', *Geophys. J. Int.*, *156*, 195–199.
Evans, H., T. Westerhold, H. Paulsen, and J. Channell (2007), Astronomical ages for Miocene polarity chrons C4Ar-C5r (9.3-11.2 Ma), and for three excursion chrons within C5n. 2n, *Earth Planet. Sci. Lett.*, *256*(3–4), 455–465, doi:10.1016/j.epsl.2007.02.001.
Fischer, A., T. Herbert, G. Napoleone, I. Silva, and M. Ripepe (1991), Albian pelagic rhythms (Piobbico core), *J. Sediment. Res.*, *61*(7), 1164–1172.
Gradstein, F., J. Ogg, and A. Smith (2004), *A Geologic Time Scale 2004*, Cambridge Univ. Press, Cambridge, U. K.
Gradstein, F., J. Ogg, M. Schmitz, and G. Ogg (2012), *The Geologic Time Scale 2012*, Elsevier, Amsterdam.
Hays, J. D., J. Imbrie, and N. J. Shackleton (1976), Variations in the Earth's orbit: Pacemaker of the ice ages, *Science*, *194*, 1121–1132, doi:10.1126/science.194.4270.1121.
Hilgen, F. (1991), Astronomical calibration of Gauss to Matuyama sapropels in the Mediterranean and implication for the geomagnetic polarity time scale, *Earth Planet. Sci. Lett.*, *104*(2–4), 226–244, doi:10.1016/0012-821X(91)90206-W.
Hilgen, F., W. Krijgsman, and J. Wijbrans (1997), Direct comparison of astronomical and 40Ar/39Ar ages of ash beds: Potential implications for the age of mineral dating standards, *Geophys. Res. Lett.*, *24*(16), 2043–2046, doi:10.1029/97GL02029.
Hilgen, F., H. Brinkhuis, and W. Zachariasse (2006), Unit stratotypes for global stages: The Neogene perspective, *Earth Sci. Rev.*, *74*(1–2), 113–125, doi:10.1016/j.earscirev.2005.09.003.
Hilgen, F., L. Lourens, and J. Van Dam (2012), The Neogene period, in *The Geologic Time Scale 2012*, pp. 923–978, Elsevier, Amsterdam.
Hilgen, F. J., W. Krijgsman, C. G. Langereis, L. J. Lourens, A. Santarelli, and W.-J. Zachariasse (1995), Extending the astronomical (polarity) time scale into the Miocene, *Earth Planet. Sci. Lett.*, *136*(3–4), 495–510, doi:10.1016/0012-821X(95)00207-S.
Hilgen, F. J., H. Abdul Aziz, W. Krijgsman, I. Raffi, and E. Turco (2003), Integrated stratigraphy and astronomical tuning of the Serravallian and lower Tortonian at Monte dei Corvi (middle-upper Miocene, northern Italy), *Palaeogeogr. Palaeoclimatol. Palaeoecol.*, *199*(3–4), 229–264, doi:10.1016/S0031-0182(03)00505-4.
Hilgen, F. J., et al. (2014), Stratigraphic continuity and fragmentary sedimentation: The success of cyclostratigraphy as part of integrated stratigraphy, in *Strata and Time: Probing the Gaps in Our Understanding*, *Geol. Soc. London Spec. Publ.*, 404, doi:10.1144/SP404.12.
Hinnov, L. (2000), New perspectives on orbitally forced stratigraphy, *Annu. Rev. Earth Planet. Sci.*, *28*(1), 419–475, doi:10.1146/annurev.earth.28.1.419.
Hinnov, L., and J. Park (1998), Detection of astronomical cycles in the stratigraphic record by frequency modulation (FM) analysis, *J. Sediment. Res.*, *68*(4), 524–539.
Holbourn, A., W. Kuhnt, M. Schulz, and H. Erlenkeuser (2005), Impacts of orbital forcing and atmospheric carbon dioxide on Miocene ice-sheet expansion, *Nature*, *438*(7067), 483–487, doi:10.1038/nature04123.
Huybers, P. (2007), Glacial variability over the last two million years: An extended depth-derived age model, continuous obliquity pacing, and the Pleistocene progression, *Quat. Sci. Rev.*, *26*, 37–55, doi:10.1016/j.quascirev.2006.07.013.
Huybers, P. (2011), Combined obliquity and precession pacing of late Pleistocene deglaciations, *Nature*, *480*, 229–232, doi:10.1038/nature10626.
Huybers, P., and O. Aharonson (2010), Orbital tuning, eccentricity, and the frequency modulation of climatic precession, *Paleoceanography*, *25*, PA4228, doi:10.1029/2010PA001952.
Huybers, P., and C. Wunsch (2004), A depth-derived Pleistocene age model: Uncertainty estimates, sedimentation variability, and nonlinear climate change, *Paleoceanography*, *19*, PA1028, doi:10.1029/2002PA000857.
Huybers, P., and C. Wunsch (2005), Obliquity pacing of the late Pleistocene glacial terminations, *Nature*, *434*, 491–494, doi:10.1038/nature03401.
Kuiper, K., A. Deino, F. Hilgen, W. Krijgsman, P. Renne, and J. Wijbrans (2008), Synchronizing rock clocks of Earth history, *Science*, *320*(5875), 500–504, doi:10.1126/science.1154339.
Kuiper, K., J. Wijbrans, and F. Hilgen (2005), Radioisotopic dating of the Tortonian Global Stratotype Section and Point: Implications for intercalibration of 40Ar/39Ar and astronomical dating methods, *Terra Nova*, *17*(4), 385–398, doi:10.1111/j.1365-3121.2005.00625.x.
Laskar, J. (1990), The chaotic motion of the solar system: A numerical estimate of the size of the chaotic zones, *Icarus*, *88*(2), 266–291, doi:10.1016/0019-1035(90)90084-M.
Laskar, J., F. Joutel, and F. Boudin (1993), Orbital, precessional, and insolation quantities for the Earth from −20 Myr to +10 Myr, *Astron. Astrophys.*, *270*(1–2), 522–533.
Laskar, J., P. Robutel, F. Joutel, M. Gastineau, A. Correia, and B. Levrard (2004), A long-term numerical solution for the insolation quantities of the Earth, *Astron. Astrophys.*, *428*(1), 261–285, doi:10.1051/0004-6361:20041335.
Laskar, J., A. Fienga, M. Gastineau, and H. Manche (2011), La2010: A new orbital solution for the long-term motion of the Earth, *Astron. Astrophys.*, *532*, A89, doi:10.1051/0004-6361/201116836.
Lisiecki, L. E. (2010), Links between eccentricity forcing and the 100,000-year glacial cycle, *Nat. Geosci.*, *3*, 349–352, doi:10.1038/ngeo828.
Lourens, L., F. Hilgen, N. Shackleton, J. Laskar, and D. Wilson (2004), The Neogene period, in *A Geologic Time Scale*, pp. 409–440, Cambridge Univ. Press, Cambridge, U. K.
Lourens, L., J. Becker, R. Bintanja, F. Hilgen, E. Tuenter, R. van de Wal, and M. Ziegler (2010), Linear and non-linear response of late Neogene glacial cycles to obliquity forcing and implications for the Milankovitch theory, *Quat. Sci. Rev.*, *29*(1), 352–365, doi:10.1016/j.quascirev.2009.10.018.
Lourens, L. J., A. Antonarako, A. A. M. Van Hoof, C. Vergnaud-Grazzini, and W. J. Zachariasse (1996a), Evaluation of the Plio-Pleistocene astronomical timescale, *Paleoceanography*, *11*, 391–413, doi:10.1029/96PA01125.
Lourens, L. J., F. Hilgen, I. Raffi, and C. Vergnaud-Grazzini (1996b), Early Pleistocene chronology of the Vrica section (Calabria, Italy), *Paleoceanography*, *11*(6), 797–812, doi:10.1029/96PA02691.
Lourens, L. J., R. Wehausen, and H. Brumsack (2001a), Geological constraints on tidal dissipation and dynamical ellipticity of the Earth over the past three million years, *Nature*, *409*(6823), 1029–1033, doi:10.1038/35059062.
Lourens, L. J., et al. (2001b), Ti/Al ratios of ODP Site 160-967, available from the PANGAEA Data Publisher for Earth and Environmental Science.

Luterbacher, H., J. Ali, H. Brinkhuis, F. Gradstein, J. Hooker, S. Monechi, J. Ogg, J. Powell, U. Röhl, and A. Sanfilippo (2004), The Paleogene period, in *A Geologic Time Scale*, pp. 384–408, Cambridge Univ. Press, Cambridge, U. K.

Malinverno, A., E. Erba, and T. D. Herbert (2010), Orbital tuning as an inverse problem: Chronology of the early Aptian oceanic anoxic event 1a (Selli Level) in the Cismon APTICORE, *Paleoceanography*, *25*, PA2203, doi:10.1029/2009PA001769.

Meyers, S. R. (2012), Seeing red in cyclic stratigraphy: Spectral noise estimation for astrochronology, *Paleoceanography*, PA3228, doi:10.1029/2012PA002307.

Meyers, S. R. (2014), Astrochron: An R Package for Astrochronology. [Available at http://cran.r-project.org/package=astrochron.]

Meyers, S. R., and L. A. Hinnov (2010), Northern Hemisphere glaciations and the evolution of Plio-Pleistocene climate noise, *Paleoceanography*, *25*, PA3207, doi:10.1029/2009PA001834.

Meyers, S. R., and B. B. Sageman (2007), Quantification of deep-time orbital forcing by average spectral misfit, *Am. J. Sci.*, *307*, 773–792, doi:10.2475/05.2007.01.

Meyers, S. R., B. B. Sageman, and L. A. Hinnov (2001), Integrated quantitative stratigraphy of the Cenomanian-Turonian Bridge Creek Limestone Member using Evolutive Harmonic Analysis and stratigraphic modeling, *J. Sediment. Res.*, *71*, 627–643.

Meyers, S. R., B. B. Sageman, and M. Pagani (2008), Resolving Milankovitch: Consideration of signal and noise, *Am. J. Sci.*, *308*, 770–786.

Meyers, S. R., S. E. Siewert, B. S. Singer, B. B. Sageman, D. J. Condon, J. D. Obradovich, B. R. Jicha, and D. A. Sawyer (2012a), Intercalibration of radioisotopic and astrochronologic time scales for the Cenomanian/Turonian boundary interval, Western Interior Basin, U.S.A., *Geology*, *40*, 7–10, doi:10.1130/G32261.1.

Meyers, S. R., B. B. Sageman, and M. A. Arthur (2012b), Obliquity forcing of organic matter accumulation during Oceanic anoxic event 2, *Paleoceanography*, *27*, PA3212, doi:10.1029/2012PA002286.

Neeman, B. (1993), Orbital tuning of Paleoclimate records: A reassessment, Lawrence Berkeley Laboratory Report, LBNL- 39572, 37 pp.

Paillard, D. (2001), Glacial cycles: Toward a new paradigm, *Rev. Geophys.*, *39*(3), 325–346, doi:10.1029/2000RG000091.

Paillard, D., L. Labeyrie, and P. Yiou (1996), Macintosh program performs time-series analysis, *Eos Trans.*, *77*(39), 379, doi:10.1029/96EO00259.

Pälike, H., N. Shackleton, and U. Röhl (2001), Astronomical forcing in late Eocene marine sediments, *Earth Planet. Sci. Lett.*, *193*(3-4), 589–602, doi:10.1016/S0012-821X(01)00501-5.

Pälike, H., J. Laskar, and N. Shackleton (2004), Geologic constraints on the chaotic diffusion of the solar system, *Geology*, *32*(11), 929–932, doi:10.1130/G20750.1.

Pälike, H., J. Frazier, and J. Zachos (2006a), Extended orbitally forced palaeoclimatic records from the equatorial Atlantic Ceara Rise, *Quat. Sci. Rev.*, *25*(23–24), 3138–3149, doi:10.1016/j.quascirev.2006.02.011.

Pälike, H., R. Norris, J. Herrle, P. Wilson, H. Coxall, C. Lear, N. Shackleton, A. Tripati, and B. Wade (2006b), The heartbeat of the Oligocene climate system, *Science*, *314*(5807), 1894–1898, doi:10.1126/science.1133822.

Raffi, I., J. Backman, E. Fornaciari, H. Pälike, D. Rio, L. Lourens, and F. Hilgen (2006), A review of calcareous nannofossil astrobiochronology encompassing the past 25 million years, *Quat. Sci. Rev.*, *25*(23–24), 3113–3137, doi:10.1016/j.quascirev.2006.07.007.

Renne, P., A. Deino, R. Walter, B. Turrin, C. Swisher III, T. Becker, G. Curtis, W. Sharp, and A. Jaouni (1994), Intercalibration of astronomical and radioisotopic time, *Geology*, *22*(9), 783–786, doi:10.1130/0091-7613(1994)022<0783:IOAART>2.3.CO;2.

Rial, J. (1999), Pacemaking the ice ages by frequency modulation of Earth's orbital eccentricity, *Science*, *285*(5427), 564, doi:10.1126/science.285.5427.564.

Rial, J., and C. Anaclerio (2000), Understanding nonlinear responses of the climate system to orbital forcing, *Quat. Sci. Rev.*, *19*(17–18), 1709–1722, doi:10.1016/S0277-3791(00)00087-1.

Ripepe, M., and A. Fischer (1991), Stratigraphic rhythms synthesized from orbital variations, in *Sedimentary Modeling: Computer Simulations and Methods for Improved Parameter Definition*, *Kansas State Geol. Surv. Bull.*, vol. 233, edited by K. Franseen et al., pp. 335–344, Lawrence, Kansas.

Rivera, T. A., M. Storey, C. Zeeden, F. J. Hilgen, and K. Kuiper (2011), A refined astronomically calibrated 40Ar/39Ar age for Fish Canyon sanidine, *Earth Planet. Sci. Lett.*, *311*(3–4), 420–426, doi:10.1016/j.epsl.2011.09.017.

Robertson, A. H. F., K.-C. Emeis, C. Richter, and A. Camerlenghi (Eds.) (1998), *Proc. ODP, Sci. Results*, vol. 160, Ocean Drilling Program, College Station, Tex., doi:10.2973/odp.proc.sr.160.1998.

Ruddiman, W., M. Raymo, and A. McIntyre (1986), Matuyama 41,000-year cycles: North Atlantic Ocean and northern hemisphere ice sheets, *Earth Planet. Sci. Lett.*, *80*(1), 117–129, doi:10.1016/0012-821X(86)90024-5.

Shackleton, N. (2000), The 100,000-year ice-age cycle identified and found to lag temperature, carbon dioxide, and orbital eccentricity, *Science*, *289*(5486), 1897–1902, doi:10.1126/science.289.5486.1897.

Shackleton, N., and S. Crowhurst (1997), Sediment fluxes based on an orbitally tuned time scale 5 Ma to 14 Ma, Site 926, in *Proceedings of the Ocean Drilling Program*, *Sci. Results*, *154*, 69–82.

Shackleton, N., T. Hagelberg, and S. Crowhurst (1995), Evaluating the success of astronomical tuning: Pitfalls of using coherence as a criterion for assessing pre-Pleistocene timescales, *Paleoceanography*, *10*(4), 693–697, doi:10.1029/95PA01454.

Shackleton, N., M. Hall, I. Raffi, L. Tauxe, and J. Zachos (2000), Astronomical calibration age for the Oligocene-Miocene boundary, *Geology*, *28*(5), 447–450, doi:10.1130/0091-7613(2000)28<447:ACAFTO>2.0.CO;2.

Shackleton, N. J., W. B. Curry, C. Richter, and T. J. Bralower (Eds.) (1997), *Proc. ODP, Sci. Results*, vol. 154, Ocean Drilling Program, College Station, Tex., doi:10.2973/odp.proc.sr.154.1997.

Spearman, C. (1904), The proof and measurement of association between two things, *Am. J. Psychol.*, *15*(1), 72–101.

Taner, M. T. (1992), In: Attributes revisited (Technical Report, Rock Solid Images, Inc), url: http://rocksolidimages.com/pdf/attrib_revisited.htm.

Tiedemann, R., M. Sarnthein, and N. Shackleton (1994), Astronomic timescale for the Pliocene Atlantic d18O and dust flux records of Ocean Drilling Program Site 659, *Paleoceanography*, *9*(4), 619–638, doi:10.1029/94PA00208.

Turco, E., A. Bambini, L. Foresi, S. Iaccarino, F. Lirer, R. Mazzei, and G. Salvatorini (2002), Middle Miocene high-resolution calcareous plankton biostratigraphy at Site 926 (Leg 154, equatorial Atlantic Ocean): Palaeoecological and palaeobiogeographical implications, *Geobios*, *35*, 257–276, doi:10.1016/S0016-6995(02)00064-5.

Valero, L., M. Garcés, L. Cabrera, E. Costa, and A. Sáez (2014), 20 Myr of eccentricity paced lacustrine cycles in the Cenozoic Ebro Basin, *Earth Planet. Sci. Lett.*, *408*, 183–193, doi:10.1016/j.epsl.2014.10.007.

Vandenberghe, N., F. Hilgen, and R. Speijer (2012), The Paleogene period, in *The Geologic Time Scale 2012*, pp. 855–921, Elsevier, Amsterdam.

van der Laan, E., S. Gaboardi, F. J. Hilgen, and L. J. Lourens (2005), Regional climate and glacial control on high-resolution oxygenisotope records from Ain el Beida (latest Miocene, northwest Morocco): A cyclostratigraphic analysis in the depth and time domain, *Paleoceanography*, *20*, PA1001, doi:10.1029/2003PA000995.

Vaughan, S., R. J. Bailey, and D. G. Smith (2011), Detecting cycles in stratigraphic data: Spectral analysis in the presence of red noise, *Paleoceanography*, *26*, PA4211, doi:10.1029/2011PA002195.

Vaughan, S., R. J. Bailey, and D. G. Smith (2014), Cyclostratigraphy: Data filtering as a source of spurious spectral peaks, in *Strata and Time: Probing the Gaps in Our Understanding*, *Geol. Soc. London Spec. Publ.*, *404*, doi:10.1144/SP404.11.

von Dobeneck, T., and F. Schmieder (1999), Using rock magnetic proxy records for orbital tuning and extended time series analyses into the super- and sub-Milankovitch bands, in *Use of Proxies in Paleoceanography: Examples From the South Atlantic*, edited by G. Fischer and G. Wefer, pp. 601–633, Springer, New York.

Wehausen, R., and H. Brumsack (2000), Chemical cycles in Pliocene sapropel-bearing and sapropel-barren eastern Mediterranean sediments, *Palaeogeogr. Palaeoclimatol. Palaeoecol.*, *158*(3), 325–352, doi:10.1016/S0031-0182(00)00057-2.

Wendler, J. E., S. R. Meyers, I. Wendler, and J. Kuss (2014), A million-year-scale astronomical control on Late Cretaceous sea-level, *Newsl. Stratigr.*, *47*(1), 1–19, doi:10.1127/0078-0421/2014/0038.

Westerhold, T., and U. Röhl (2006), Data report: Revised composite depth records for Shatsky Rise Sites 1209, 1210, and 1211, in *Proc. ODP, Sci. Results*, vol. 198, edited by T. Bralower, I. Premoli Silva, and M. Malone, pp. 1–16, Ocean Drilling Program, College Station, Tex., doi:10.2973/odp.proc.sr.198.122.2006.

Westerhold, T., and U. Röhl (2009), High resolution cyclostratigraphy of the early Eocene–New insights into the origin of the Cenozoic cooling trend, *Clim. Past*, *5*, 309–327, doi:10.5194/cp-5-309-2009.

Westerhold, T., T. Bickert, and U. Rohl (2005), Middle to late Miocene oxygen isotope stratigraphy of ODP site 1085 (SE Atlantic): New constrains on Miocene climate variability and sea-level fluctuations, *Palaeogeogr. Palaeoclimatol. Palaeoecol.*, *217*(3–4), 205–222, doi:10.1016/j.palaeo.2004.12.001.

Westerhold, T., U. Röhl, J. Laskar, I. Raffi, J. Bowles, L. Lourens, and J. Zachos (2007), On the duration of magnetochrons C24r and C25n and the timing of early Eocene global warming events: Implications from the Ocean Drilling Program Leg 208 Walvis Ridge depth transect, *Paleoceanography*, *22*, PA2201, doi:10.1029/2006PA001322.

Westerhold, T., U. Röhl, and J. Laskar (2012), Time scale controversy: Accurate orbital calibration of the early Paleogene, *Geochem. Geophys. Geosyst.*, *13*, Q06015, doi:10.1029/2012GC004096.

Westerhold, T., U. Röhl, H. Pälike, R. Wilkens, P. A. Wilson, and G. Acton (2014), Orbitally tuned timescale and astronomical forcing in the middle Eocene to early Oligocene, *Clim. Past*, *10*, 955–973, doi:10.5194/cp-10-955-2014.

Wu, H., S. Zhang, G. Jiang, L. Hinnov, T. Yang, H. Li, X. Wan, and C. Wang (2013), Astrochronology of the Early Turonian–Early Campanian terrestrial succession in the Songliao Basin, northeastern China and its implication for long-period behavior of the Solar System, *Palaeogeogr. Palaeoclimatol. Palaeoecol.*, *385*, 55–70, doi:10.1016/j.palaeo.2012.09.004.

Zachos, J., N. Shackleton, J. Revenaugh, H. Palike, and B. Flower (2001), Climate response to orbital forcing across the Oligocene-Miocene boundary, *Science*, *292*(5515), 274–278, doi:10.1126/science.1058288.

Zeeden, C., F. Hilgen, T. Westerhold, L. Lourens, U. Röhl, and T. Bickert (2013a), Greyscale values from ODP Site 154-926 sediments, available from the PANGAEA Data Publisher for Earth and Environmental Science, doi:10.1594/PANGAEA.774388.

Zeeden, C., F. Hilgen, T. Westerhold, L. Lourens, U. Röhl, and T. Bickert (2013b), Revised Miocene splice, astronomical tuning and calcareous plankton biochronology of ODP Site 926 between 5 and 14.4 Ma, *Palaeogeogr. Palaeoclimatol. Palaeoecol.*, *369*, 430–451, doi:10.1016/j.palaeo.2012.11.009.

Zeeden, C., T. A. Rivera, and M. Storey (2014), An astronomical age for the Bishop Tuff and concordance with radioisotopic dates, *Geophys. Res. Lett.*, *41*, 3478–3484, doi:10.1002/2014GL059899.

ERRATUM

In the supporting information for the originally published version of this article, previous version of the 'testing' routine was named 'validateP', where the final function name in the 'astrochron' R package is 'testPrecession'. The supporting files have since been corrected and this version may be considered the authoritative version of record.